REPORT DOCUMENTATION PAGE

Form Approved
OMB No. 0704-0188

1. REPORT DATE *(DD-MM-YYYY)*	2. REPORT TYPE	3. DATES COVERED *(From - To)*
	Technical Paper	

4. TITLE AND SUBTITLE

5a. CONTRACT NUMBER

5b. GRANT NUMBER

5c. PROGRAM ELEMENT NUMBER
62500F

6. AUTHOR(S)

5d. PROJECT NUMBER
2308

5e. TASK NUMBER
M4S7

5f. WORK UNIT NUMBER
345382

7. PERFORMING ORGANIZATION NAME(S) AND ADDRESS(ES)

8. PERFORMING ORGANIZATION REPORT

9. SPONSORING / MONITORING AGENCY NAME(S) AND ADDRESS(ES)

Air Force Research Laboratory (AFMC)
AFRL/PRS
5 Pollux Drive.
Edwards AFB CA 93524-7048

10. SPONSOR/MONITOR'S ACRONYM(S)

11. SPONSOR/MONITOR'S NUMBER(S)

12. DISTRIBUTION / AVAILABILITY STATEMENT

Approved for public release; distribution unlimited.

13. SUPPLEMENTARY NOTES

See attached 13 papers, all with the information on this page.

14. ABSTRACT

15. SUBJECT TERMS

16. SECURITY CLASSIFICATION OF:			17. LIMITATION OF ABSTRACT	18. NUMBER OF PAGES	19a. NAME OF RESPONSIBLE PERSON
a. REPORT	b. ABSTRACT	c. THIS PAGE			Kenette Gfeller
Unclassified	Unclassified	Unclassified	A		19b. TELEPHONE NUMBER *(include area code)* (661) 275-5016

AIAA 97-2924

Spectroscopic Emission Measurements of a Pulsed Plasma Thruster Plume

Thomas E. Markusic and Ronald A. Spores
Phillips Laboratory
Edwards AFB, CA

33rd AIAA/ASME/SAE/ASEEJoint Propulsion Conference & Exhibit
July 6 - 9, 1997 / Seattle, WA

Spectroscopic Emission Measurements of a Pulsed Plasma Thruster Plume

Thomas E. Markusic and Ronald A. Spores
US Air Force Electric Propulsion Laboratory, Edwards AFB, CA

The optical emission spectra of plasmas produced by a Teflon (polytetrafluoroethylene (PTFE)) solid propellant pulsed plasma thruster (XPPT-1) were measured and analyzed. A broad temporally and spatially integrated survey of the emission from 3500 to 7500 Å is reported. It is shown that in the PPT discharge energy range surveyed (15 to 45 J), the species formed do not vary, that is. no new species are formed as the discharge energy is increased. Furthermore, relative line ratios do not vary significantly with energy, suggesting that the bulk thermodynamic properties of the discharge plasma may not be affected by changing the initial stored capacitor energy. A spatially integrated but time-resolved measurement was carried out which shows the single species emission as a function of PPT discharge time. The magnitude of the emission was found to track closely with the PPT current and depend on the discharge energy. Relative line emission intensities are used to determine the degree of excitation equilibrium and establish bounds on the plasma temperature. Spatially and temporally resolved images are used to estimate the plasma streaming velocity from time-of-flight and Doppler-shift techniques.

I. INTRODUCTION

There is presently a strong, renewed interest in Pulsed Plasma Thrusters (PPT) for a wide range of space missions. MightySat II.1[1], scheduled for a 2000 launch, will fly a PPT on-board that is designed to perform an orbit raising maneuver from an initial Space Shuttle altitude of 200 to 215 nm up to greater than 250 nm; this maneuver will extend the life of the satellite from two months to one year. The EO-1 satellite, scheduled for a 1999 launch, will be using a PPT for attitude control[2]. PPTs have the potential of fulfilling the attitude control role on a satellite at greatly reduced mass and cost. PPTs are also being considered for constellation maintenance for such missions as interferometric imaging of the Earth from space or deep space from an Earth orbit. The benefits of PPTs are its very small impulse bits ($\approx 10^{-6}$ Ns) for satellite motion, reliability, high specific impulse and overall ease of system integration. These are extremely simple devices with only one moving part, the negator spring.

Even though there are many missions where PPTs are advantageous with existing performance, the range of applications is expected to greatly increase if their overall performance can be improved. There are two broad categories of inefficiencies in pulsed plasma thrusters that limit the present performance. These include energy inefficiencies which pertain to the efficient transfer of stored capacitor energy into acceleration of the ionized propellant and propellant inefficiencies which include particulate emission and late-time vaporization[3]. The work described in this paper employs emission spectroscopy to better understand the ablation plasma formation and subsequent acceleration mechanisms in present PPTs in order to improve overall future performance. Both spatial and temporal resolution are used to record the emission spectrum produced during the arc discharge in XPPT-1, a rectangular geometry thruster described in an earlier work[3]. Investigated in this work are the identification of constituent species, temporal dependence of emission, electron temperature measurements, and exhaust velocity.

While analysis of the observed PPT emission is useful in the determination of plasma parameters, partitioning of energy, and the speed of streaming motion, it also provides a starting point for more advanced diagnostics, such as laser-induced fluorescence, by identifying electronic transitions that are active in the unperturbed plasma. In the present work we describe two emission ex-

periments which are primarily qualitative, and two that establish rough quantitative bounds on the plasma temperature and streaming velocity. The first experiment determined the atomic and molecular species present at *any time* during the PPT discharge. The second experiment showed how the production of a species depends on the instantaneous discharge current. The third experiment establishes bounds on the plasma temperature by the analysis of the distribution of upper states of a fixed specie and degree of ionization. The last experiment establishes bounds on the streaming velocity of the accelerated propellant. This is accomplished by imaging a side view of the emission gated at several times during the discharge. A second approach compares the simultaneously measured front and side view spectral lines to determine a Doppler shift in the axial emission from which the axial streaming velocity follows directly.

The PPT PTFE plasma is formed by the arc ablation and subsequent dissociation of the C_2F_4 monomer. The species observed in the present study were F, F^+, C^+, C^{++}, and C_2. Other species, such as C, were probably also present; however, these species do not have any strong lines in the wave number range surveyed.

II. EXPERIMENT

In this section the details of the equipment used in all of the experiments is described; then, a more detailed description of the four experiments performed is given. A top view of the experimental arrangement is shown in Figure 1. The vacuum chamber has three optical diagnostic access windows. It uses a single turbomolecular pump backed by a mechanical rough pump to achieve a base pressure of about 1×10^{-5} Torr.

External optics were configured to allow imaging of either the front or side view (or both simultaneously) of the thruster. The lenses were $\phi 50$ mm with f/8 which provided an image magnification of 2.5. Periscopes were used to rotate the imaging plane and, in the case of simultaneous imaging of the front and side view, to allow spatial separation of the images on the CCD array.

A Czerny-Turner mount 1.26 m SPEX 1269 spectrometer was used. Two different diffraction gratings were employed: a 1200 g/mm ruled grating blazed at 1μ, and a 2400 g/mm unblazed holographic grating. With the 1200 g/mm grating installed, the spectrometer gives a first order exit plane linear dispersion of about 6.25 Å/mm. Typical slit widths were 6-10μ.

The spectrometer output was detected by either a Princeton Instruments CCD camera (model# 576G/RBE) or a Hamamatsu photo-multiplier tube

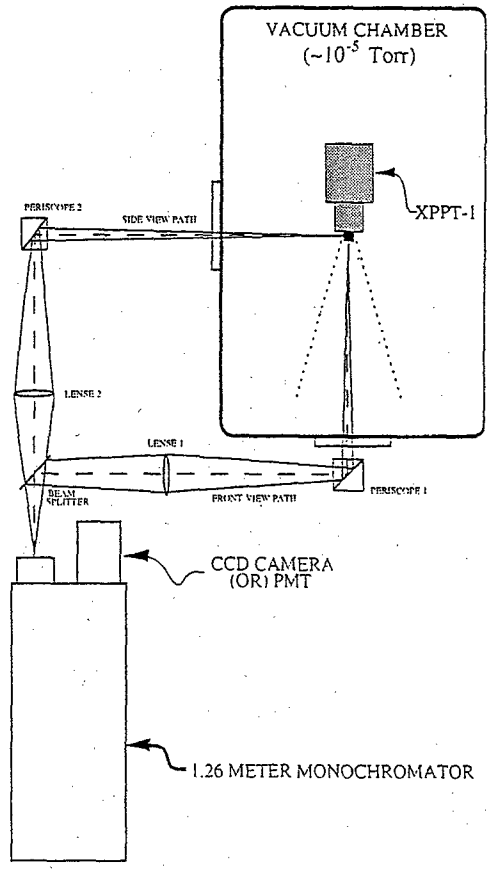

Figure 1: Schematic of apparatus for PPT emission spectroscopy.

(PMT)(model# 921). The camera has a thermoelectrically cooled, gated, and image intensified detector composed of a two-dimensional array (576×384) of 22μ pixels. The overall spectrograph/CCD system resolution was limited by the pixel size of the CCD array; the wavelength resolution was found to be 0.13 Å. About 80 Å of the optical spectrum was recorded in a single shot with the 1200 g/mm grating. The minimum gate width was 100 ns. The timing for the gate was coordinated with the PPT discharge by a Stanford Research digital delay generator. The photomultiplier tube was used to obtain continuously time resolved data. The response time of the detector used is approximately 2.2 ns. The spectrometer/CCD/PMT system spectral sensitivity was calibrated using an Oriel quartz-tungsten–halogen (QTH) lamp (model# 6334) and its published spectral irradiance[4].

A. SURVEY OF SPECTRAL LINES

An initial experiment was conducted to determine the species present in the plume at any time during the discharge. The spectrograph was scanned in 80 Å increments (the 1200 g/mm grating was used) from 3500 to 7500 Å. The optics were arranged in the front view path orientation illustrated in Figure 1. A central horizontal slice (approximately 2.5 cm wide) of the PTFE propellant face was imaged onto the spectrograph entrance slit (7μ width) and subsequently onto the CCD array. Since the XPPT-1 electrodes are 2.5 cm wide, this imaging assured that the discharge arc would be captured by the camera regardless of where it initiated or terminated. Typical XPPT-1 discharges range from fifteen to twenty-five microseconds in duration, depending on the discharge energy. The CCD gating was adjusted such that the CCD shutter was opened approximately 5 μs before the discharge, and closed approximately 75 μs after the discharge terminated (i.e. there was no current flowing). Thus, the acquired images represent a spatially and temporally integrated accounting of species present during and immediately after the discharge. Scans were performed at three different PPT discharge energies: 15 J, 25 J, and 45 J.

B. TIME RESOLVED SPECTRA

Once the strong lines had been identified, time resolved measurements were conducted. The same front view optical arrangement as in Experiment A was used; however, the CCD camera was replaced with an exit slit and a photo-multiplier tube. For each measurement, the monochromator wavelength was set to the peak intensity of a previously identified transition. The entrance and exit slits were set to 8μ and 6μ, respectively. The PMT and PPT currents were measured simultaneously and displayed and recorded on a Tektronix digital oscilloscope. Both the PMT and the PPT were triggered by a Stanford Research digital delay generator. This procedure was carried out for several lines of each specie. These measurements were also performed at three different PPT discharge energies: 15 J, 25 J, and 45 J.

C. PLASMA TEMPERATURE

The correlation of relative line intensities of members of the same species with plasma temperature was used to determine an estimate of the electron temperature. Only the carbon ion proved to have a sufficient distribution of lines to be used for such an analysis; seven C^+ lines were obtained using the CCD camera. The CCD shutter gate-open time was set to 100 ns and the gate delay was adjusted to make the CCD shutter-open-time correspond to peak PPT current; the two waveforms were monitored on the digital oscilloscope. The side-view optical setup was chosen to avoid non-uniform line distortion from the Doppler effect. The 1200 g/mm diffraction grating was used and the entire optical path was calibrated for intensity using the the QTH lamp.

D. PLASMA STREAMING VELOCITY

Two approaches were used to estimate the speed of the plasma leaving the thruster during the arc discharge phase.

The first technique used time-of-flight to track the position of the plasma front as it expanded from the solid PTFE face. The emission was imaged in the side view orientation (see Figure 1). The CCD camera shutter gate-open-time was 100 ns; the gate delay was adjusted to give "snapshots" of the plasma at various times during the discharge cycle. The resulting images then show plasma front position as a function of time, that is, plasma speed transverse to the viewing direction. The CCD camera was rotated ninety degrees to allow the maximum amount of space to be imaged (i.e. the 578 pixel direction was aligned vertically with the spectrograph entrance slit($25\ \mu$)). The spatial dimension of the CCD array was calibrated using a Mercury pen ray lamp masked to a known dimension. The lamp was placed in the thruster position and imaged back to the spectrograph entrance slit and then acquired by the CCD camera — allowing the number of CCD pixels per unit distance to be calculated. It was found that approximately seven centimeters of axial distance in front of the solid PTFE face could be imaged. Representative lines of F^+, C^+, and C^{++} were recorded at various discharge times for later analysis. All of the images were acquired with 25 J PPT discharge energies.

The second approach resolved the Doppler shift of the emitted radiation from particles moving axially away from the thruster. Both the front and side views of the thruster were imaged simultaneously. This obviated the need for exact wavelength calibration since the side-view line was assumed to have zero Doppler shift, and therefore provided an intrinsic reference point for the shifted front-view line. An Inconel beam splitter was used to image both views onto the entrance slit ($11\ \mu$). The 2400 g/mm grating was implemented to provide maximum dispersion, and the CCD camera was in the standard orientation (longer dimension in the wavelength direction). The CCD gate-open time was 100 ns, and the images were acquired at peak current (25 J discharge energy). Due to the narrow slit, short gate time, and losses in the beam splitter, only the carbon ion had sufficient intensity to be resolved.

III. RESULTS

A. SURVEY OF SPECTRAL LINES

Five species were identified by comparing the acquired emission lines with a standard reference[5]: F, F^+, C^+, C^{++}, and C_2. Figure 2 shows these lines; prominent lines are labeled to identify the corresponding specie. Some of the lines are overlapping multiplets and therefore represent averages in intensity and wavelength. The figure contains plots for three different discharge energy levels: 15 J, 25 J, and 45 J (the species are labeled only in the 15 J case). All of the plots have been calibrated to remove instrumental effects that change with wavelength or environmental conditions: intensity, wavelength, and background signal (primarily thermal). The plots represent averages over three discharge cycles.

Table 1 gives the wavelength and term designations (as found in Moore[6]) of the upper and lower electronic states of the dominant transitions (i.e. those with the greatest emissivities). Also apparent in the plots are the rotational and vibrational bands of molecular carbon—the so-called Swan bands[7].

The three plots in Figure 2 are structurally very similar. The only apparent difference is a modest increase in relative fluorine emission at higher PPT discharge energies. Since a change in relative emissivity is directly related to a change in relative species population, the figure shows that increasing discharge energy leads to a slight increase in the relative population of F^+ while the C^+ and C^{++} lines show little variation (note: the ionization potentials of C^+, F, and C are 24.38 eV, 17.42 eV, and 11.26 eV, respectively[5]). Two conclusions can immediately be reached. First, increasing PPT discharge energy does not lead to (at least in the energy range of the present survey) a significant production of more highly ionized species such as F^{++} and C^{+++} (the ionization potentials of F^+ and C^{++} are 34.97 eV and 47.89 eV, respectively[5]). Since the additional discharge energy is not going into the production of more highly ionized species, it must be accounted for elsewhere. One possiblility is that increased stored energy leads to the the ablation and ionization of *more* material, rather than the deposition of the additional energy into a *constant* amount of matter. A second possibility is that the degree of ionization (i.e. the total percentage of liberated PTFE that is ionized) is increased. These conclusions are further supported by the fact that the relative line intensity ratios between members of the same specie do not change significantly as the discharge energy is increased. This implies that the electron temperature remains remains fairly constant regardless of the discharge energy.

Two species are conspicuously absent in the spectrum: C and CF. These species are undoubtedly present; however, their strongest lines occur in the UV and IR—regions that were outside of the present survey.

B. TIME RESOLVED SPECTRA

The time dependence of emission was recorded for C^+, C^{++}, F, and F^+ at three different discharge energies and is shown in Figure 3. The specific lines used to produce the plots were as follows: 4267.26 Å for C^+, 4647.42 Å for C^{++}, 6856.03 Å for F, and 3847.09 Å for F^+. These lines were chosen because they gave the best signal to noise ratio. Other lines gave qualitatively similar results with reduced signal.

Table 1: Term and level designations of dominant transitions in the PPT discharge.

Specie	Emission Line [Å]	Lower Level	Upper Level
C^+	3918.98	$3p\ ^2P^\circ_{1/2}$	$4s\ ^2S_{1/2}$
C^+	3920.69	$3p\ ^2P^\circ_{3/2}$	$4s\ ^2S_{1/2}$
C^+	4267.00	$3d\ ^2D_{3/2}$	$4f\ ^2F^\circ_{5/2}$
C^+	4267.26	$3d\ ^2D_{5/2}$	$4f\ ^2F^\circ_{5/2}$
C^+	5889.77	$3d\ ^2D_{5/2}$	$4p\ ^2P^\circ_{3/2}$
C^+	5891.59	$3d\ ^2D_{3/2}$	$4p\ ^2P^\circ_{3/2}$
C^+	6578.05	$3s\ ^2S_{1/2}$	$3p\ ^2P^\circ_{1/2}$
C^+	6582.88	$3s\ ^2S_{1/2}$	$3p\ ^2P^\circ_{3/2}$
C^+	7231.32	$3p\ ^2P^\circ_{1/2}$	$3d\ ^2D_{3/2}$
C^+	7236.42	$3p\ ^2P^\circ_{3/2}$	$3d\ ^2D_{5/2}$
C^{++}	4647.42	$3s\ ^3S_1$	$3p\ ^3P^\circ_2$
C^{++}	4650.25	$3s\ ^3S_1$	$3p\ ^3P^\circ_1$
F	6239.65	$3s\ ^4P_3$	$3p\ ^4S^\circ_2$
F	6348.51	$3s\ ^4P_2$	$3p\ ^4S^\circ_2$
F	6856.03	$3s\ ^4P^\circ_3$	$3p\ ^4D_4$
F	7037.47	$3s\ ^2P_2$	$3p\ ^2P^\circ_2$
F	7127.89	$3s\ ^2P_1$	$3p\ ^2P^\circ_1$
F	7754.70	$3s\ ^2P_2$	$3p\ ^2D^\circ_3$
F^+	3501.45	$3p\ ^5P_1$	$3d\ ^5D^\circ_0$
F^+	3847.09	$3s\ ^5S^\circ_2$	$3p\ ^5P_3$
F^+	4024.73	$3s\ ^3S^\circ_1$	$3p\ ^3P_2$
F^+	4103.51	$3p\ ^3P_3$	$3d\ ^3D^\circ_3$
F^+	4246.23	$4f\ ^5F_3$	$3d\ ^5D^\circ_2$

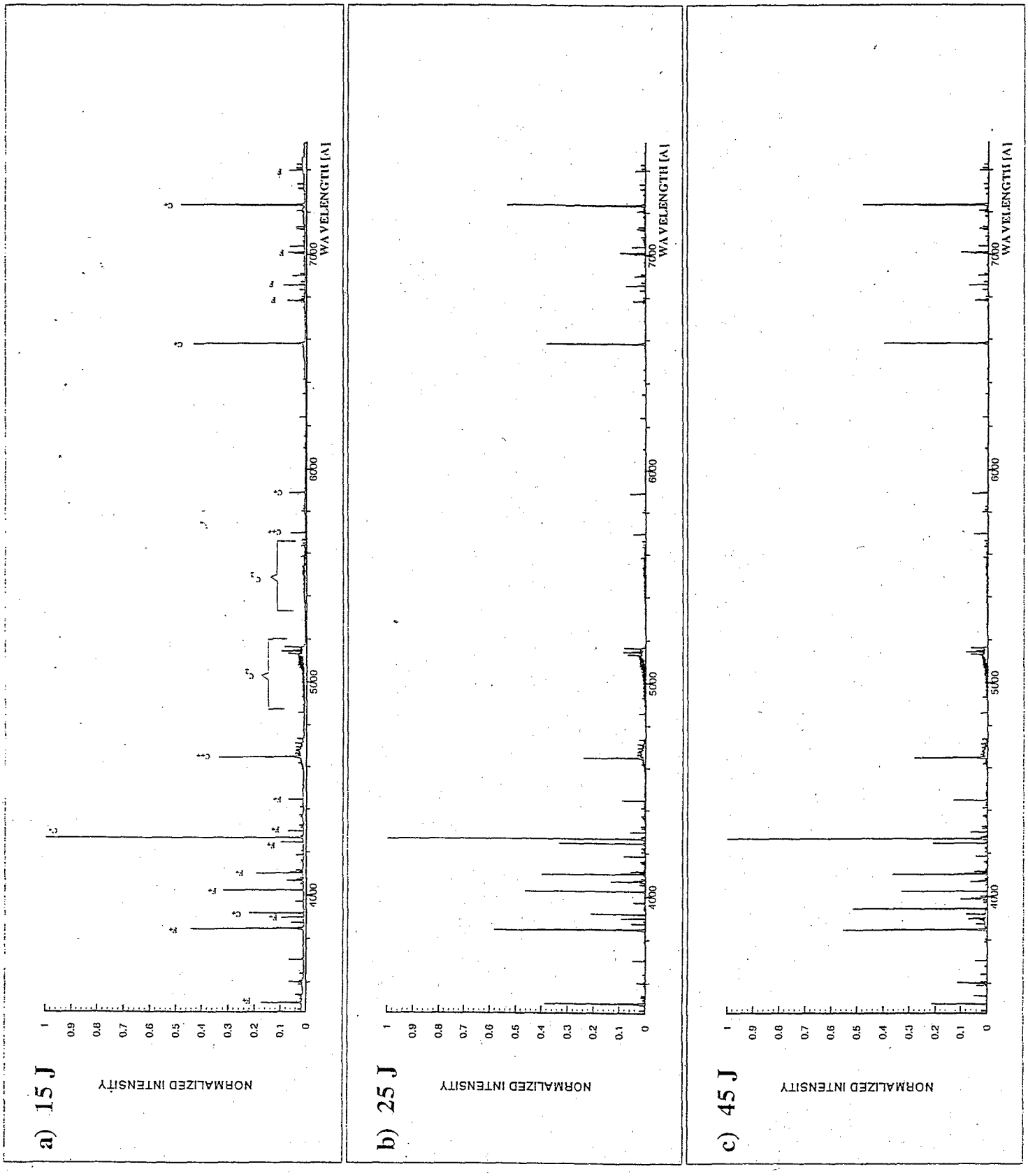

Figure 2: Survey of PPT optical emission spectrum from 3500 to 7500 Å for three different discharge energies: a) 15 J, b)25 J, c) 45 J.

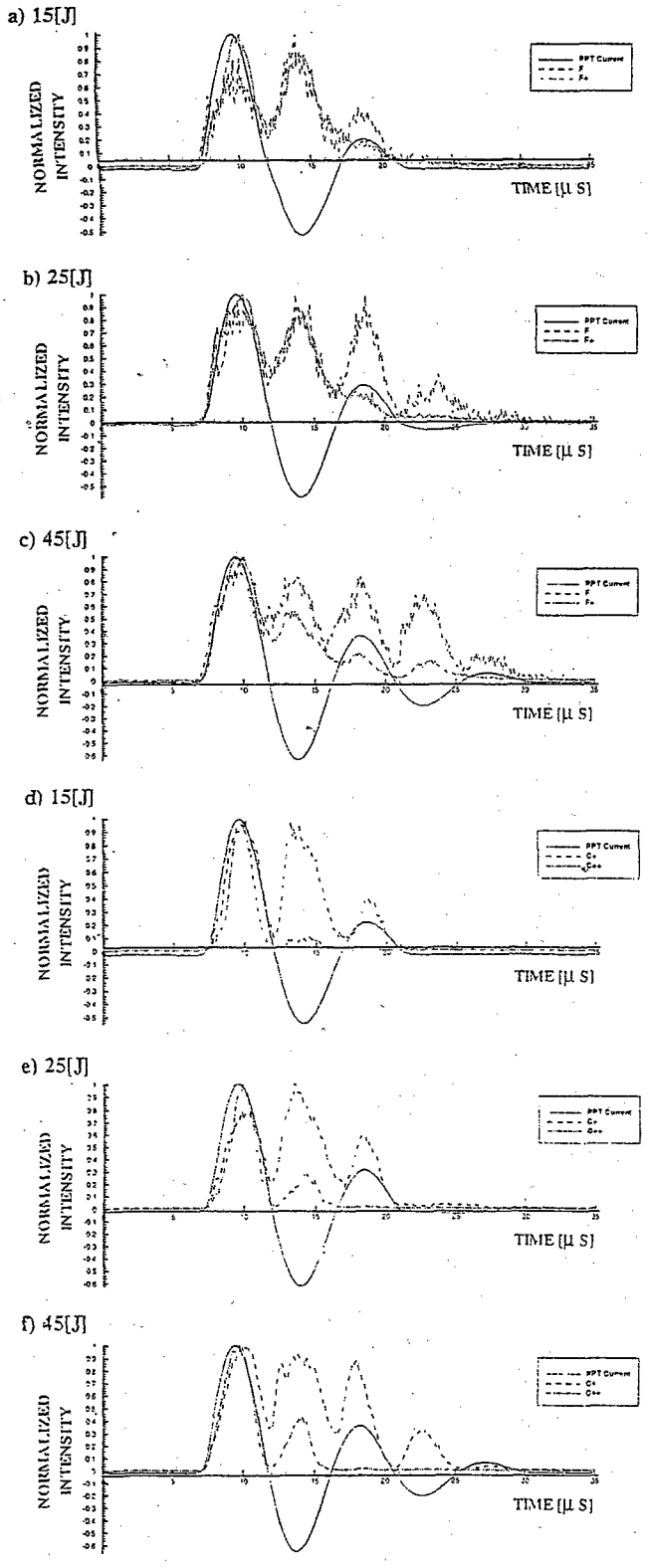

Figure 3: PPT emission as a function of discharge time and energy.

The illustrated data represent averages taken over ten discharge cycles. All data was normalized, and therefore is in arbitrary units (i.e. no correlation should be made between absolute intensities of different species). The peak current in each case was: 9.75 kA at 15 J, 12.5 kA at 25 J, and 18.5 kA at 45 J discharge energy.

All of the data show that the emission tracks closely with the current. The peak emission occurs near peak current—lagging the current by less than a microsecond. The delay in peak emission may be explained if we consider the PPT as a one-sided ablation controlled arc[8]. The observed delay could then be attributed to the propellant transit time between being liberated from the solid PTFE face and being entrained in the current sheet (i.e. the solid face and arc are separated by a thin vapor layer).

From Figure 3 it is clear that the emission profiles are affected by the discharge energy in two ways. First, increasing the discharge energy results in about one half-cycle of additional current swing per ten Joules of additional energy (e.g. the 15 J discharge terminates after one cycle while the 45 J discharge terminates after two and one half-cycles). The additional current oscillations provide an opportunity for the plasma to "re-ignite" and emit radiation. Also, higher discharge energies give higher peak currents and, in turn, higher populations of emitters.

General trends are evident in Figure 3. As the current "rings down" the discharge supports decreasing populations of the more highly ionized species. This is most apparent in Figure 3d), where the C^{++} emission is almost nonexistent in the second half-cycle. However, C^{+} and F seem to defy this trend, at least in the first discharge cycle. For example, in Figure 3e) the C^{+} emission is actually twenty-five percent greater in the second half-cycle than in the first half-cycle, even though the current is only sixty percent of its peak value. This suggests that, in the second half-cycle. the current carrying electrons have insufficient energy to produce a sizeable population of the species with higher ionization potentials (F^{+} and C^{++}); therefore, a greater proportion of the discharge energy is available to create the more weakly excited species F and C^{+}; thus, the emission of these species is maintained near peak levels in both the first and second half-cycles.

C. PLASMA TEMPERATURE

When the conditions of a plasma are such that local thermodynamic equilibrium (LTE) applies, the populations of the bound states follow a Boltzmann distribution[9]. It is uncertain whether the the prevailing conditions in a transient discharge such as the PPT reach a state of thermal equilibrium, or if measured excitation equilibrium neces-

sarily implies complete local thermodynamic equilibrium (CLTE). In the present work, the assumption of LTE is made *a priori*, and explored by referring to the measured data.

Relative emissivities of singly ionized carbon will be used to calculate electron temperature. The lines must be well resolved for accurate emissivities (ϵ_{mn}), and the transition probabilities (A_{mn}) must be known. Since the populations of the excited states are given by the Boltzmann distribution, Equation 1 describes their relative emissivity:

$$\ln\left(\frac{\epsilon_{mn}}{g_m A_{mn} \nu_{mn}}\right) = \ln\frac{N}{Z} - \frac{E_m}{kT} \quad , \qquad (1)$$

where, for a transition from upper state m to lower state n, ν_{mn} is the frequency, E_m and g_m are the energy and degeneracy of the upper state, respectively, k is the Boltzmann constant, and T is the temperature. A plot of the quantity on the left-hand-side of Equation 1 versus E_m has a slope of -1/kT. Therefore, the temperature can be obtained without N, the total number density, or Z, the partition function.

For experimental data, the application of this technique is only accurate when the distribution of measured upper state energies (i.e. the spetral lines which represent transitions from these states) is comparable to the ambient electron temperature. Of the dominant transitions listed in Table 1, only C^+ exhibits a sufficient distribution of upper states, and has satisfactorily resolved lines, to be useful in the present analysis. The distribution of upper states listed in Table 2 spans approximately 4.6 eV in energy. We can therefore legitamately expect to have the resolution to analyse temperatures ranging from 1 to 10 eV.

Seven well-resolved transitions of C^+ were available. The upper level degeneracies and transition probabilities are given in Table 2. Only relative emissivities are required and these were obtained by numerical integration of the CCD output. An eighth line (C^+ 4267.26) that was not "well resolved" is included. Since this line dominates the spectrum (see Figure 2), its inclusion in the present analysis is necessary. The line is not well resolved because it overlaps the C^+ 4267.0 line with the available instrumental resolution. The C^+ 4267.26 line may be included in the temperature analysis by assuming that it is in excitation equilibrium with the C^+ 4267.0. In this case, the relative emissivities of the two lines can be found from Equation 1:

$$\frac{\epsilon_{4267.0}}{\epsilon_{4267.26}} \approx \frac{g_{4267.0}\ A_{4267.0}\ \nu_{4267.0}}{g_{4267.26}\ A_{4267.26}\ \nu_{4267.26}} \quad . \qquad (2)$$

It should be noted that this separating of the two overlapping carbon ion lines in no way invalidates their inclusion in the Boltzmann plot since both lines have the same upper state.

Table 2: Parameters for electron temperature determination.

Specie	Emission Line [Å]	E_m (cm^{-1})	g_m	A_{mn} ($X10^8\ s^{-1}$)
C^+	3918.98	157 234	2	0.636
C^+	3920.69	157 234	2	1.27
C^+	4267.26	168 978	8	2.38
C^+	5889.77	162 525	4	0.315
C^+	6578.05	131 736	4	0.363
C^+	6582.88	131 724	2	0.362
C^+	7231.32	145 549	4	0.352
C^+	7236.42	145 551	6	0.422

A plot of the left-hand-side of Eq. 1 using the experimentally acquired lines given in Table 2 is shown in Figure 4, where each of the points represents data averaged over five shots. A least squares linear fit is also illustrated. The linear fit indicates an electron temperature of 1.4±0.2 eV (≈ 16000 K). The experimental data does not fall perfectly on the straight line, nor does it deviate in any ordered manner; therefore, no strong argument for or against LTE can be made. However, since the deviation from linearity is not large, we can safely assume that the calculated tempera-

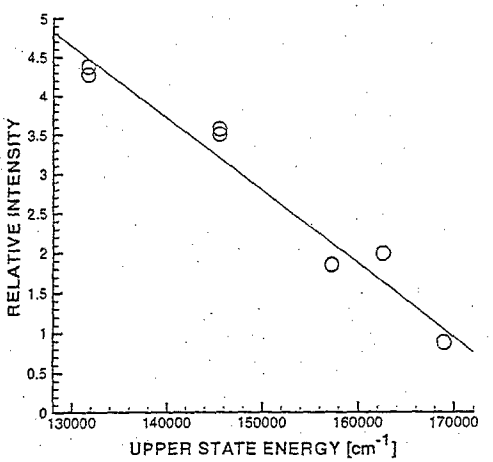

Figure 4: Relative emissivities corrected for degeneracy and radiative rate vs. energy of upper state.

ture is representative of the mean thermal energy of the electrons.

D. PLASMA STREAMING VELOCITY

The velocity of the ejected plasma varies with position and time in the PPT. In this section we determine the speed of the propellant immediately after it is liberated from the solid PTFE surface during the first half-cycle of current flow.

The first approach used was time-of-flight. Figure 5 shows a typical current trace. Four times are indicated by the arrows on the horizontal axis of the graph: times A, B, C, and D (0.1 μs, 1.6 μs, 3.68 μs, and 4.68 μs, respectively) . These times correspond to CCD "snapshots" that are illustrated in Figure 6. The horizontal axis in Figure 6 is the axial distance from the propellant face. The physical position and extent of the PPT electrodes is is illustrated above the curves.

Plots A, B, C, and D show the emission from C^+ as the plasma expands downstream early in the first half-cycle of the discharge. To determine the rate of expansion (i.e. the speed) we must establish where the plasma "front" is in each case. This position is somewhat subjective; therefore, any reasonable measure that is consistently applied to all cases will be valid. We choose to define the plasma front as that position where the degrading emission reaches $1/e$ of its peak value. These points are indicated in Figure 6 by the vertical dashed lines that intersect each curve. Combining the temporal information from Figure 5 with the spatial information from Figure 6 we can compute the speed of the expanding front.

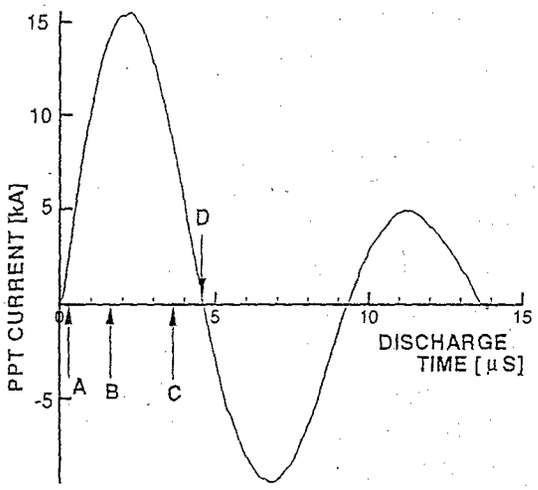

Figure 5: Typical PPT current trace with CCD image timing locations on horizontal axis.

Comparing the emission at points A and B we find $v_{front} \approx 8.1$ km/s, B and C give $v_{front} \approx 15.5$ km/s, and C and D give $v_{front} \approx 14.7$ km/s. Apparently the carbon ions continue to accelerate between times A, B, and C and have reached a terminal speed of approximately 15 km/s between times C and D. Similar measurements were made on C^{++} and F^+; the speeds were found to be approximately 14.1 km/s and 15.9 km/s, respectively.

A second diagnostic to determine streaming velocity is the Doppler shift of emitted radiation. The speed v of an emitting particle moving relative to a stationary observer is given by,

$$v = c\left(\frac{\lambda_o - \lambda}{\lambda_o}\right) \qquad (3)$$

where c is the speed of light, λ_o is the rest wavelength, and λ is the measured wavelength.

Both the side and front view of the thruster were simultaneously imaged onto the entrance slit. This allows for an intrinsic reference point for Doppler shift measurements. More specifically, the measurement of the Doppler shift does not depend on wavelength calibration of the spectrometer since the side view of the thruster provides a simultaneous (and presumably unshifted) reference line.

Figure 7 shows the C^+ 6578.05 Å line acquired in the simultaneous front/side arrangement. Two peaks separated by approximately 0.21 Å are ev-

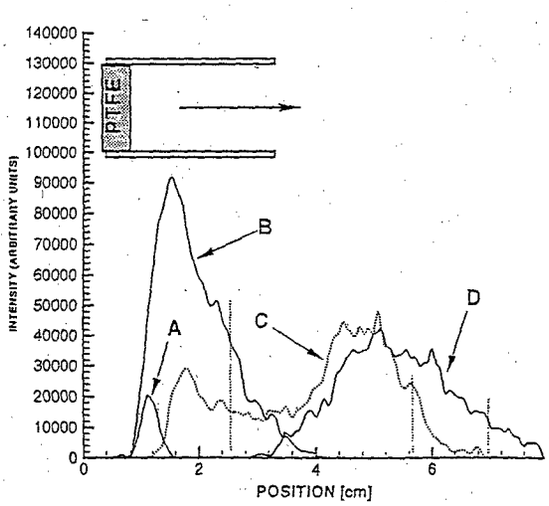

Figure 6: Axial spatial distribution of emission at four different times. The PPT position and electrode extent is illustrated above the graph.

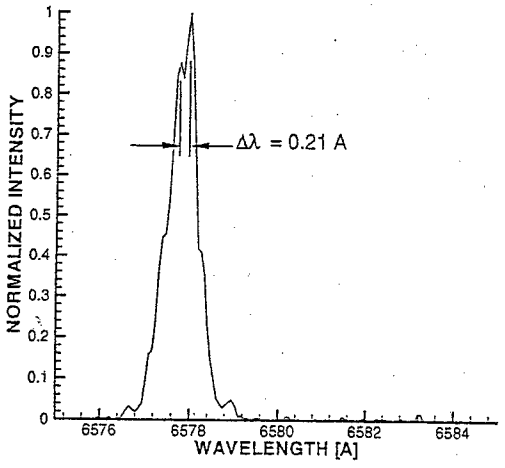

Figure 7: C^+ emission line representing simultaneous front and side-view images.

ident. From Equation 3 we compute the particle speed to be 9.6 ±5.5 km/s, where the margin of error is a result of the maximum spectrometer resolution. Only the carbon ion line had sufficient intensity to be resolved with the narrow entrance slit and short gate width used in this experiment.

The Doppler shift illustrated in Figure 7 was measured at 2.1 μs (see Figure 6). The time-of-flight estimated speed in this region (between points B and C) was found to be between 8.1 km/s and 15.1 km/s. Therefore, the time-of-flight and Doppler shift techniques have been shown to give, within the intrinsic system uncertainty, comparable estimates of the plasma streaming speed.

IV. DISCUSSION

The primary goal of this study was to determine the constituent particles that are present in a PTFE PPT discharge, and when these particles form relative to the current pulse. Secondarily, approximate quantitative estimates of the plasma temperature and streaming velocity were desired. In this section, sources of error in the acquisition and interpretation of the experimental data are explored. These sources of error are especially pertinent to the validity of the quantitative sections of the paper. Without careful application of tomographic techniques to resolve phenomena spatially, emission spectroscopy provides only qualitative information or, at best, allows one to establish bounds on the value of a spatially integrated experimental parameter.

Calculations were carried out to estimate the optical thickness of the plasma. The absorption coefficient due to inverse Bremsstrahlung K_ν is given by Eq. 4, where Z is the average charge (one) and ν is the frequency of the light [11]

$$K_\nu = 3.69 \times 10^8 (Z N_e^2)/(T^{1/2}\nu^3) \quad . \qquad (4)$$

Losses due to stimulated emission are assumed to be insignificant under our conditions and the correction term for it has not been included. At $N_e = 1 \times 10^{17}$ cm^{-3}, $T_e = 16000$k, and $\lambda = 5500$ Å, Eq. 4 yields $K_\nu = 1.8 \times 10^{-4}$ cm^{-1}. Since the plasma extent is a few centimeters, the weak absorption ($1/K_\nu = 55.6$ m) due to inverse Bremsstrahlung does not affect our quantitative spectroscopy.

The data presented in the spectral survey and time resolved emission sections of the paper are essentially qualitative. The data were compiled as averages over several discharges and therefore remove any non-periodic phenomena.

In reference to the plasma temperature section of the paper, a very important question must be posed: "Where exactly in the plasma is the electron temperature 1.4 eV?" The acquired CCD images represent spatially integrated emission; the collected light is coming from many different layers within the plasma which undoubtedly have different temperatures. We make the assumption that the preponderance of the collected light is generated from within or very near the arc column, and the quoted temperature therefore applies only to that region of the plasma.

The time-of-flight data and analysis should be an accurate representation of the initial plasma expansion. The C^+ lifetimes are short in comparison to the CCD camera gate width. The plasma translation is less than 0.3 mm while the camera shutter is open. Two other possible sources of error exist in the time-of-flight data. We assumed that the regions that were emitting light represented the spatial extent of the gas that had been accelerated from the thruster; however, if processes such as recombination were to deplete the leading edge of the expanding front of emitters, we would not observe emission from that region. Consequently, our estimate of the speed would be lower than the actual exhaust speed of the thruster. Second, the emission from the arc region of the plasma may overwhelm the signal coming from other regions of the plasma. This would have the effect of not allowing the accurate determination of axial extent of the plasma. This effect would be especially important in the early stages of the discharge, such as those indicated as points A and B in Figure 6, and would lead to the calculation of the arc propagation speed rather than the plasma streaming speed. This may, in part, explain the difference in the calculated speeds between point A,B and B,C. The Doppler shift data is not, by itself, an accurate measurement. Clearly the two lines are not completely resolved (Rayleigh's criterion is not satisfied). However, accounting for the spectroscopic

system resolution, the Doppler measurement does allow us to establish an upper bound on the carbon ion speed of about 15 km/s. In short, while the measurement does not provide an accurate quantitative value of the speed, it does establish bounds on the speed which support the time-of-flight findings. Also, as was mentioned in the temperature discussion, the lack of spatial resolution in the measurement implies that we are measuring the Doppler shift of a distribution of velocities; we are integrating emission from particles that are at the face of the PTFE (with presumably low speeds) through particles that have reached their terminal speeds. Consequently, the Doppler shift data may be dominated by emission from slow moving particles near the PTFE surface, which does not accurately represent the final distribution of velocities.

Line-width and line-shape analysis is a common technique used to extract plasma parameters. This type of analysis was not conducted in the present study for two reasons. First, for the estimated plasma conditions, the contributions to line broadening due to Doppler broadening and the Stark effect are found to be of comparable magnitude. Therefore, it would be difficult to deconvolve the two effects in a given line. Second, the estimated Doppler and Stark widths are smaller than the available resolution of the spectroscopic system.

Measurements similar to those in the present work were carried out by earlier researchers[12]. In particular, exhaust velocities were determined using time-of-flight and Doppler shift techniques. The range of axial speeds found in that study were: 11.0 to 28.0 km/s for C^+. 13.0 to 42.0 km/s for C^{++}, and 5.0 to 20.0 km/s for F^+. The values found in the present study agree with the earlier findings, albeit on the low side of the range.

V. CONCLUSION

The species present in a PTFE PPT plume have been identified; further, the composition of the PPT exhaust plasma has been shown to be independent of discharge energy in the regions surveyed. Temporal resolution of the emission has qualitatively illustrated the dependence of emission on discharge energy and current. Local thermodynamic equilibrium was assumed to yield an lectron temperature of 1.4±0.2 eV ($\approx$ 16000 K). Spatially and temporally resolved images were obtained to place bounds on the axial plasma streaming speed. It was found that the terminal speed of the ionized species of the plasma is between 14 to 16 km/s after the first half-cycle of the discharge.

More accurate quantitative data will require spatial resolution of the discharge plasma. XPPT-1, a rectangular geometry thruster, is not a favorable design on which to perform such experiments. However, a new generation of coaxial geometry thrusters are under development at the USAF Electric Propulsion Laboratory. This axisymetric geometry will be amenable to Abel inversion techniques to fully spatially resolve the discharge plasma behavior.

References

[1] J. LeDuc, D. Bromaghim, T. Peterson, *Mission Planning, Hardware Development, and Ground Testing for the Pulsed Plasma Thruster (PPT) Space Demonstration on MightySat II.1* . AIAA-97-2777, 33rd Joint Propulsion Conference, Seattle Wa, July 7-9, 1997.

[2] Cassady, R.J., Myers, R.M., and Osborne, R.D. *Pulsed Plasma Thrusters for Spacecraft Attitude Control.* JANNAF, Albequerque, N.M., December, 1996.

[3] G. Spanjers, K. McFall, F. Gulczinski III. R. Spores, *Investigation of Propellant Inefficiencies in a Pulsed Plasma Thruster.* AIAA-96-2723, 32nd Joint Propulsion Conference, Lake Buena Vista, Fl, July 1-3, 1996.

[4] Oriel Corporation(1994), *Light Sources, Monochromators, Spectrographs, Detectors, Fiber Optics Vol. II.*

[5] Weast, R.C. *CRC Handbook of Chemistry and Physics.* CRC Press, 1989.

[6] Moore, C.E. *Tables of Spectra of Hydrogen, Carbon, Nitrogen, and Oxygen Atoms and Ions.* CRC Press, 1993.

[7] Pearse, R.W.B., and Gaydon, A.G. *The Identification of molecular Spectra.* Chapman and Hall, 1976.

[8] Ruchti, C.B., and Niemeyer, L. *Ablation Controlled Arcs.* Transactions on Plasma Science, Vol. PS-14, No.4, August 1986.

[9] Auciello, O., and Flamm, D.L. *Plasma Diagnostics Volume 1.* Academic Press, Inc., 1989.

[10] Demtroder, W., *Laser Spectroscopy.* Springer-Verlag, 1988.

[11] Bekefi, G., *Principals of Laser Plasmas.* Wiley, 1976.

[12] Vondra, R.J., Thomasson, K.I., Solbes, A., *Exhaust Velocity Studies of a Solid Teflon Pulsed Plasma Thruster.* J. Spacecraft 9,61 (1972).